Comprehensive study of solar conditions in Mozambique: the effect of trade winds on solar components

N.I. Nijegorodov [a,*], K.R.S. Devan [a], H. Simao [b], R. Mabbs [c]

[a] *Physics Department, University of Botswana, Private Bag 0022, Gaborone, Botswana*
[b] *Departamento de Fisica, Universidade Pedagogica, P.O. Box 4040, Maputo, Mozambique*
[c] *Chemistry Department, University of Arizona, Tucson, AZ 85721-0041, USA*

Received 13 July 2002; accepted 24 January 2003

Abstract

A new algorithm to simulate all solar components and optimum slopes, β_{opt}, based on new models for direct normal beam and diffuse radiation and an analytical model to predict β_{opt}, developed at the University of Botswana is applied for complete study of solar conditions in Mozambique. The components of solar radiation depend to a large extent on the number of h of sunshine. However, it is obvious that cloud-cover is determined mainly by the prevailing trade winds, which carry moisture and rain clouds. This is of especial concern in coastal areas. In the current work, hourly, I, daily, H and monthly mean, H components of solar radiation and the optimum slopes of a north–south aligned collector are simulated and analyzed for 21 synoptic stations in Mozambique. Monthly mean daily direct normal, $\bar{H}_{bn}$ solar radiation maps are plotted for December and June and discussed. It is found that, to a great extent, isoinsolation curves are determined by the prevailing trade winds, mountain chains and coastal conditions. Plotted maps of annual mean daily direct normal and global solar radiation also show tremendous dependence on the prevailing winds. Several special locations in Mozambique with quite high or very low solar radiation components are pointed out and the reasons explained.

* Corresponding author. Tel.: +267-355-2113; fax: +267-585097.
E-mail address: nijegoni@mopipi.ub.bw (N.I. Nijegorodov).

Nomenclature

A	Altitude in meters above sea level
A_i	Daily anisotropy index defined as H_b/H_0
b	Empirical coefficient to calculate H_d for partially cloudy weather
C	Daily diffuse fraction defined as H_d/H_{bn}
C_d	Diffuse fraction, defined as I_d/I_{bn}
D	Day
D_O	Thickness of ozone layer
D_1	Daily diffuse fraction defined as H_d/H_g
f, f_1	Correction factors in the computation of diffuse radiation
H_b	Daily beam radiation, MJ m^{-2} on a horizontal surface
$\bar{H}_b$	Monthly mean daily beam radiation, MJ m^{-2} on a horizontal surface
$\bar{H}_b^y$	Annual mean daily beam radiation, MJ m^{-2}
H_{bn}	Daily normal beam radiation, MJ m^{-2}
$\bar{H}_{bn}$	Monthly mean daily normal beam radiation, MJ m^{-2}
$\bar{H}_{bn}^y$	Annual mean daily normal beam radiation, MJ m^{-2}
H_d	Daily diffuse radiation, MJ m^{-2}
$\bar{H}_d$	Monthly mean diffuse radiation, MJ m^{-2}
$\bar{H}_d^y$	Annual mean daily diffuse radiation, MJ m^{-2}
H_{ef}	Effective thickness of the atmosphere
H_g	Daily global radiation, MJ m^{-2}
$\bar{H}_g$	Monthly mean global radiation, MJ m^{-2}
$\bar{H}_g^y$	Annual mean daily global radiation, MJ m^{-2}
H_r	Sunrise hour
H_s	Sunset hour
H_0	Daily extraterrestrial radiation, MJ m^{-2} on a horizontal surface
H_t	Daily total radiation, MJ m^{-2} on a tilted surface
$\bar{H}_t$	Monthly mean total radiation, MJ m^{-2} on a tilted surface
I_b	Hourly beam radiation, W m^{-2} on a horizontal surface
I_{bn}	Hourly normal beam radiation, W m^{-2}
I_d	Hourly diffuse radiation, W m^{-2}
I_g	Hourly global radiation, W m^{-2}
I_t	Hourly total radiation, W m^{-2} on a tilted surface
I_r	Hourly ground reflected radiation, W m^{-2}
I_S	Solar constant
K_T	Daily clearness index
$\bar{K}_T$	Monthly mean clearness index
$\bar{K}_T^y$	Annual mean clearness index
M	Month
$\bar{M}$	Mean molecular mass of air
m	Current air mass
m_n	Air mass at noon

m_0	Air mass for θ_z=0°
N_C	Moles of CO_2 in the vertical column of air
N_S	Total number of moles in the vertical column of air
N_W	Moles of H_2O in the vertical column of air
P_w	Pressure of water vapour
RH	% relative humidity
S	Hours of sunshine
S_{max}	Duration of day
T	Temperature in °C
V	Visibility
W_S	Sunset hour angle for a horizontal surface
Z	Daily diffuse fraction defined as H_d/H_b
β	Slope (°), facing North negative, facing South positive
β_{opt}	Optimum slope (°) of an absorber plate
β_{opt}	Monthly mean optimum slope
β^y_{opt}	Annual mean optimum slope
δ	Solar declination (°), South negative
γ	Surface azimuth angle (°), East negative
ϕ	Latitude (°), South negative
ρ	Ground albedo
θ	Angle of incidence of sun's rays on a tilted surface
θ_z	Zenith angle

1. Introduction

The Republic of Mozambique is located on the eastern coast of Southern Africa between the latitudes 10°12′ and 26°52′ and longitudes 30°12′ and 40°51′E. Its total area is 799,380 km^2, including 13,000 km^2 of inland lakes and rivers. Mozambique shares borders to the north with the United Republic of Tanzania, to the west with the Republics of Malawi, Zambia, Zimbabwe and South Africa (from north to south, respectively) and to the south with the Kingdom of Swaziland. On the eastern side of the country the Indian Ocean coast stretches over a distance of 2470 km. The climate of Mozambique is determined by coastal conditions, the prevailing trade winds and the mountain chains of Manica (central province), Maravia–Angonia (in the west of the central region), Chire–Namuli, Maniamba and Libombos (in Maputo province). The prevailing trade winds (easterlies) over Mozambique are shown in Fig. 1. In June–July the easterlies blow from the Indian Ocean and determine the climate of not only Mozambique, but also of Malawi and the eastern province of Zambia. In December–January two streams of trade winds meets at the so called Intertropical Convergence Zone (ITCZ).

A large percentage of the population of Mozambique live in remote, thinly populated rural areas where no power is available from the national grid and where oil

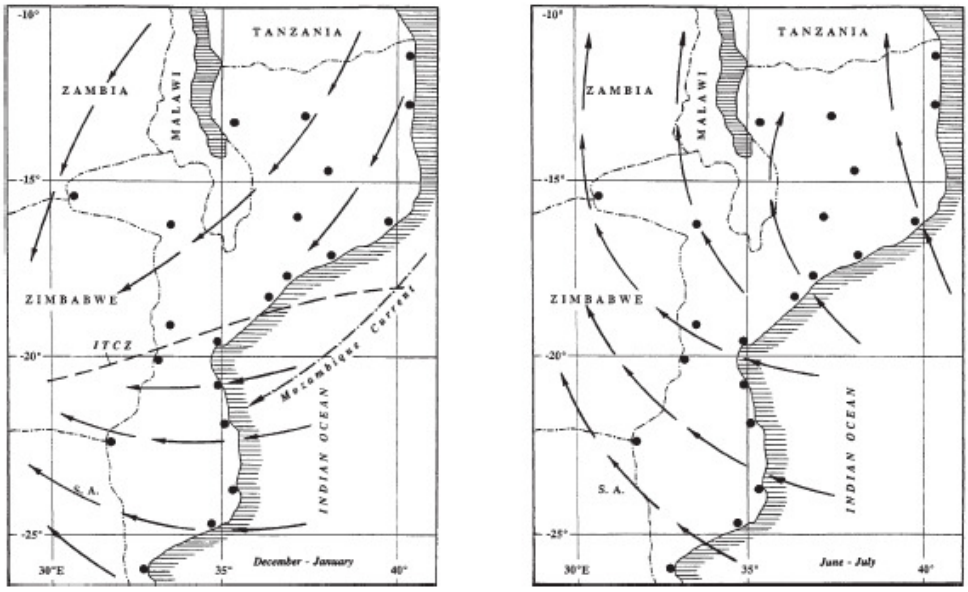

Fig. 1. Prevailing trade winds (easterlies) blowing over Mozambique in December–January (left) and June–July (right).

or coal products cannot be delivered economically. Some areas of Mozambique even lack wood for fuel due to the climatic conditions. However, Mozambique has excellent solar conditions with an average of 7–9 h of sunshine per day throughout the country. Hence, it is obvious that the power requirements in rural areas of Mozambique can be met, to a large extent, by the utilization of solar energy. Unfortunately, the solar conditions in Mozambique have been very poorly studied. Investigation of the monthly mean solar radiation components available in Mozambique is an important problem. Without knowledge of the monthly mean solar radiation it is impossible to design the size and estimate the cost and efficiency of a solar device [1]. The efficiency of solar devices such as plain solar collectors and PV-arrays depends on the angle of tilt and hence, investigation of monthly and annual mean optimum slopes for Mozambique is also an important task [2–11].

In this paper we aim to show, by simulation and comparison with data gathered at various synoptic stations, the dependence of the solar radiation components on the geographical conditions pertaining to Mozambique. The study will then be extended to determine optimum conditions of use for solar collectors and PV-arrays in this country, factors which should be useful for power generation in a remote, rural areas of the country.

2. Brief explanation of the algorithm

The new algorithm [12] developed by Nijegorodov at the University of Botswana to simulate the instantaneous, hourly, daily and monthly mean direct normal, diffuse

and global components of solar radiation and to predict daily mean and monthly mean optimum slopes is based on four major articles published in the Renewable Energy Journal [11,13–15]. The algorithm developed allows simulation of all solar radiation parameters if a slope, β, is known. If β is not known the program simulates β_{opt}. β_{opt} is found by maximizing the daily total insolation on a tilted surface with respect to tilt angle, i.e.:

$$\left[\frac{\mathrm{d}}{\mathrm{d}\beta}(H_T)\right]/\beta_{opt} = 0. \tag{1}$$

A schematic representation of the algorithm is given in Fig. 2. The solar constant, I_S is considered to be 1367 W/m^2 [1]. Input data are: T temperature, RH relative humidity, S h of sunshine, V visibility and D_O the thickness of the ozone layer. These parameters can be daily mean, if the solar components are simulated for a particular day, or monthly mean daily if monthly mean daily components are simulated for the Julian days, Jan 17, Feb 16, Mar 16, Apr 15, May 15, June 11, July 17, Aug 16, Sep 15, Oct 15, Nov 14, Dec 10.

If visibility and the thickness of the ozone layer are not known, standard values can be used (V=23 km and D_O=0.34 cm) [16,17]. Location and date input data are: ϕ latitude, A altitude, D date and M month. The third set of input data are: γ surface azimuth angle, β slope and ρ ground albedo. If all input data are available the following constants can be computed: P_w pressure due to water vapour, N_s total number of moles in the vertical column of air, N_c number of moles of carbon dioxide, N_w number of moles of water vapour, H_{ef} effective thickness of the atmosphere, $\bar{M}$ mean molecular weight of air, δ declination, W_s sunset hour angle, H_r sunrise hour, H_s sunset hour, $S_{\max}$ duration of a day, m_0 is mass for θ_z=0, m_n air mass at noon. Subsequently, the following variables are computed: m current air mass, θ current angle of incidence of the suns rays on the tilted absorber plate, Cos θ_z cosine of the current zenith angle, f and f_1 are two correction factors necessary in the computation of the diffuse fraction [14], defined as C_d=I_d/I_{bn}. The formulae required to compute the above constants and variables are given in [15]. Next, instantaneous or hourly parameters of solar radiation are computed: I_{bn} direct beam radiation, I_b beam radiation on horizontal, I_d diffuse radiation, I_r ground reflected radiation and I_t total solar radiation. The procedure to compute I_{bn} is thoroughly explained in [15] and that for I_d is given in [14]. Following these, daily or monthly mean daily solar parameters ($\bar{H}_{bn}$,$\bar{H}_b$,$\bar{H}_d$,$\bar{H}_r$ and $\bar{H}_t$) can be computed for clear cloudless and partially cloudy weather. In order to compute the daily diffuse radiation for partially cloudy weather the following formula was used;

$$H'_d = \frac{H_d}{S_{\max}}[S + b(S_{\max} - S)] \tag{2}$$

where b is an empirical parameter which gives the relationship between the daily diffuse fractions for partially cloudy and clear cloudless weather. For Southern African climatic conditions it was found that b should be equal to 1.6. The procedure and all necessary formulae required to compute the optimum slope, β_{opt} are given

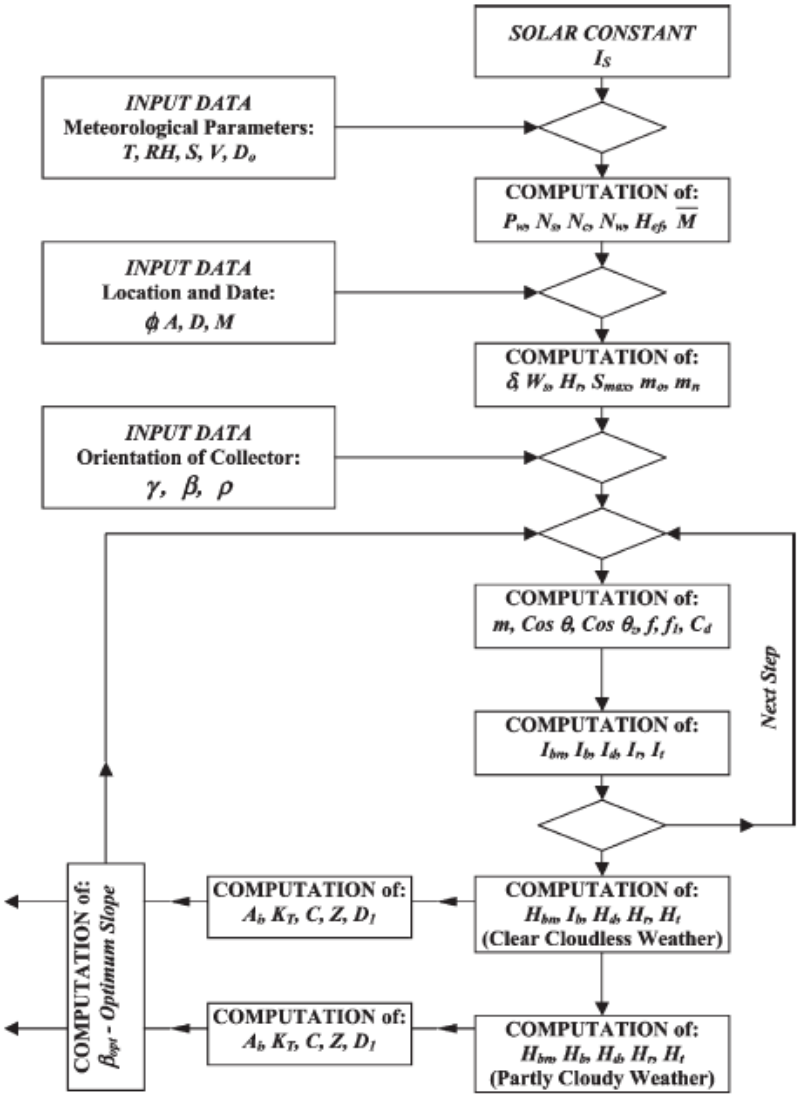

Fig. 2. Schematic representation of the algorithm to simulate hourly, daily and monthly mean daily solar radiation components and optimum slopes (all notations are given in the nomenclature).

in [11]. The remaining symbols in Fig. 2 are: A_i anisotropy index, C diffuse fraction defined as H_d/H_{bn} and Z diffuse fraction defined as H_d/H_b and D_1 diffuse fraction defined as H_d/H_g. All notations used are shown in the nomenclature.

3. Application of the algorithm

The algorithm developed is applied in this paper to study monthly mean and annual mean daily solar radiation components and monthly and annual mean optimum slopes

in Mozambique. The locations of the synoptic stations of Mozambique for which the meteorological parameters were available, are shown in Fig. 3. The altitude, A is given in meters above sea level. An example of simulation of monthly mean daily and annual daily solar components and optimum slopes is given in Table 1 (for the Maputo observatory). The median monthly temperatures, also shown in Table 1, were calculated as follows;

$$T = \frac{T_{\max} + T_{\min}}{2}. \tag{3}$$

Clearness indices, $\bar{K}_T$ were also simulated. The simulated solar radiation parameters

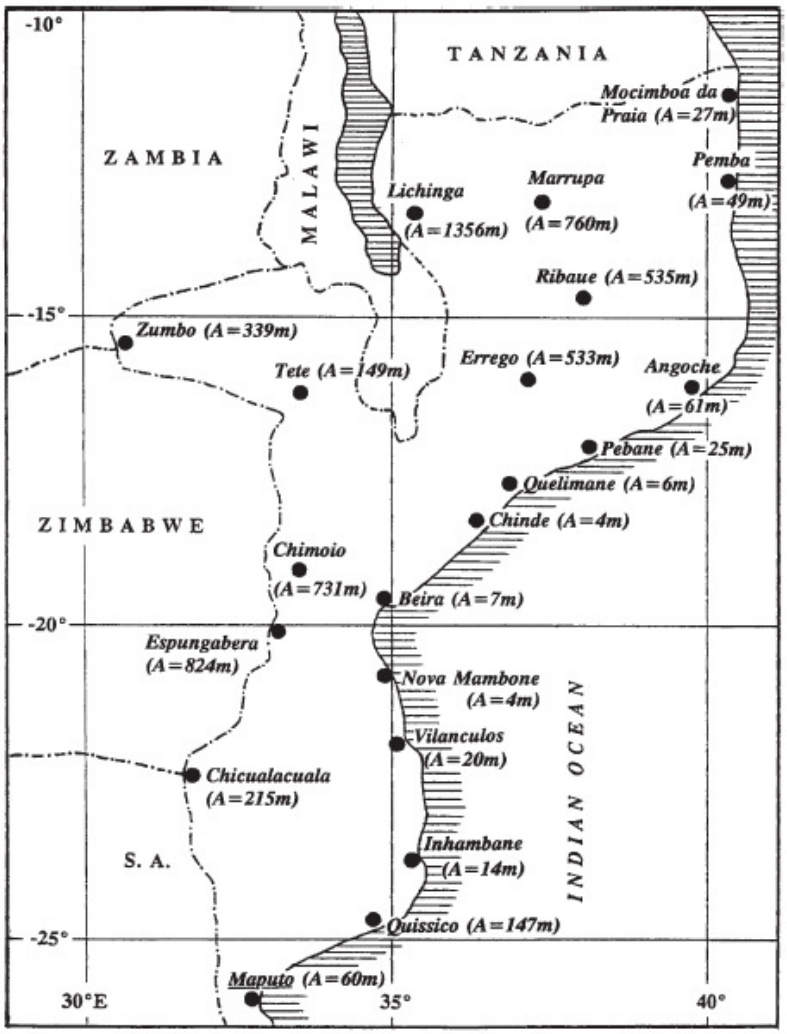

Fig. 3. Names, locations and altitudes of 21 Mozambican synoptic stations.

Table 1
Simulated monthly mean daily solar radiation parameters, clearness indices and optimum slopes for Maputo synoptic station

Solar and meteorological parameters			Month												Annual avg
			Jan	Feb	Mar	Apr	May	June	July	Aug	Sep	Oct	Nov	Dec	
Monthly	Clear, cloudless weather	$\overline{H}_{bn}$	33.2	31.4	29.3	26.7	25.0	24.1	24.7	26.9	29.2	31.4	33.3	33.9	29.1
mean		$\overline{H}_d$	4.17	3.92	3.58	3.16	2.83	2.67	2.75	3.08	3.46	3.85	4.14	4.24	3.49
daily		$\overline{H}_g$	28.3	26.2	23.4	19.2	15.8	14.2	15.0	18.2	22.4	25.8	28.2	28.9	22.1
radiation		$\overline{K}_T$	0.661	0.658	0.661	0.658	0.667	0.675	0.678	0.686	0.687	0.675	0.672	0.666	0.670
(MJ/m^2),		β_{opt}	3.9	−8.8	−24.2	−40.1	−51.2	−55.8	−53.8	−45.2	−30.7	−13.4	0.08	7.1	−29.5
cloudness	Partly cloudy weather	$\overline{H}_{bn}$	19.3	19.6	18.8	17.8	19.8	19.4	19.9	20.4	19.0	16.9	16.6	18.5	18.8
index		$\overline{H}_d$	5.04	4.66	4.22	3.68	3.12	2.93	3.02	3.46	4.07	4.74	5.18	5.21	4.11
and		$\overline{H}_g$	19.0	18.6	16.9	14.3	13.4	12.2	12.8	14.9	16.4	16.6	17.1	18.6	15.9
optimum		$\overline{K}_T$	0.404	0.429	0.442	0.457	0.541	0.557	0.558	0.533	0.464	0.387	0.359	0.385	0.460
slope (°)		β_{opt}	3.7	−8.4	−23.2	−39.1	−50.6	−55.2	−53.3	−44.6	−29.7	−12.7	0.8	6.7	−29.3
Monthly mean meteorological data		T/°C	25.8	25.8	25.1	23.7	21.5	19.4	19.2	20.2	21.5	22.7	24.0	25.1	22.8
		RH (%)	68	68	67	66	63	60	61	62	66	70	70	69	66
		S/h	7.8	8.0	7.8	7.6	8.5	8.4	8.5	8.4	7.7	6.8	6.6	7.4	7.8

for the Maputo observatory were compared with experimental data obtained over several years at this station. Such comparison showed that the error in the simulated values of direct beam radiation is ±4%, for the simulation of global radiation this is ±6% and the error limits in the simulation of diffuse radiation is within ±12%. For example, for June (Maputo station) experimental values of $\bar{H}_{bn}$, $\bar{H}_d$ and $\bar{H}_g$ are 19.6, 3.29 and 12.9 MJ/m^2. The corresponding simulated values are 19.4, 2.93 and 12.2 MJ/m^2. For December experimental values are 18.4, 6.26 and 19.3 MJ/m^2 and corresponding data are 18.5, 5.91 and 18.6 MJ/m^2. The same limits of error have been observed for Gaborone, Botswana. The low accuracy in the simulation of $\bar{H}_d$ is explained by the following. $\bar{H}_d$ is affected to a large extent by the visibility but, monthly mean visibility data are not available. Hence, the standard visibility (23 km) was used in all simulations even though visibility can vary over a large range.

The error limits in the simulation of the optimum slopes for a north–south aligned absorber plate (either a flat plane collector or a PV-panel) is within 0.5°.

Simulation of monthly mean daily solar radiation components and monthly mean optimum slopes, β_{opt} were actually carried out for 30 synoptic stations from Mozambique, Malawi and the Eastern province of Zambia. For this purpose the algorithm developed was used.

The simulated results for the 21 Mozambique synoptic stations have been analyzed and are presented in the form of maps of monthly mean daily direct beam radiation for December and June (Fig. 4), of annual mean daily direct beam and global radiation (Fig. 5) and of monthly mean optimum slopes for December and June (Fig. 6). Annual mean daily parameters and annual optimum slopes are presented in Table 2.

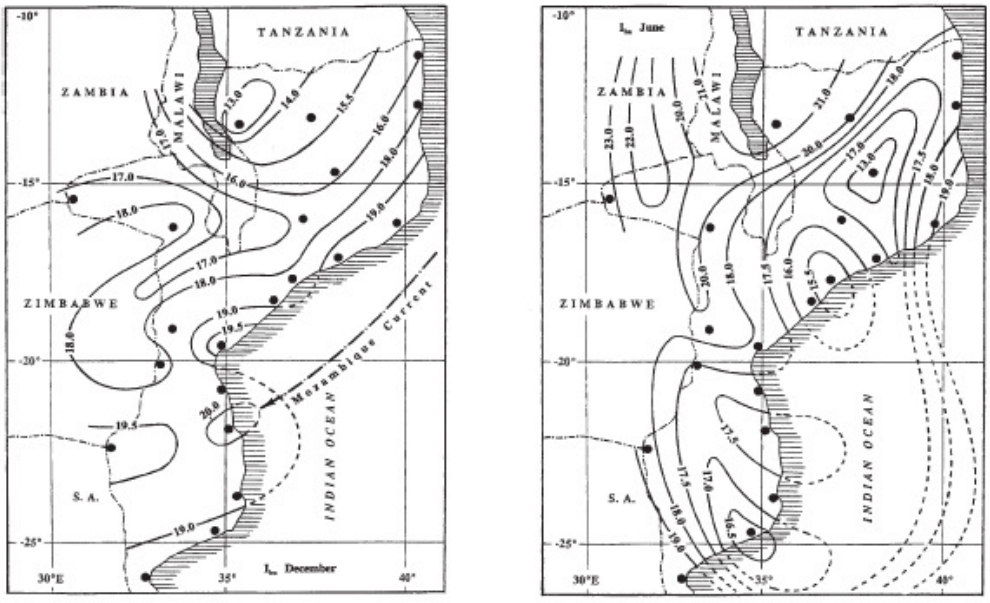

Fig. 4. Maps of monthly mean daily direct beam normal radiation (values indicated are in MJ m^{-2}) for December (left) and June (right) for Mozambique.

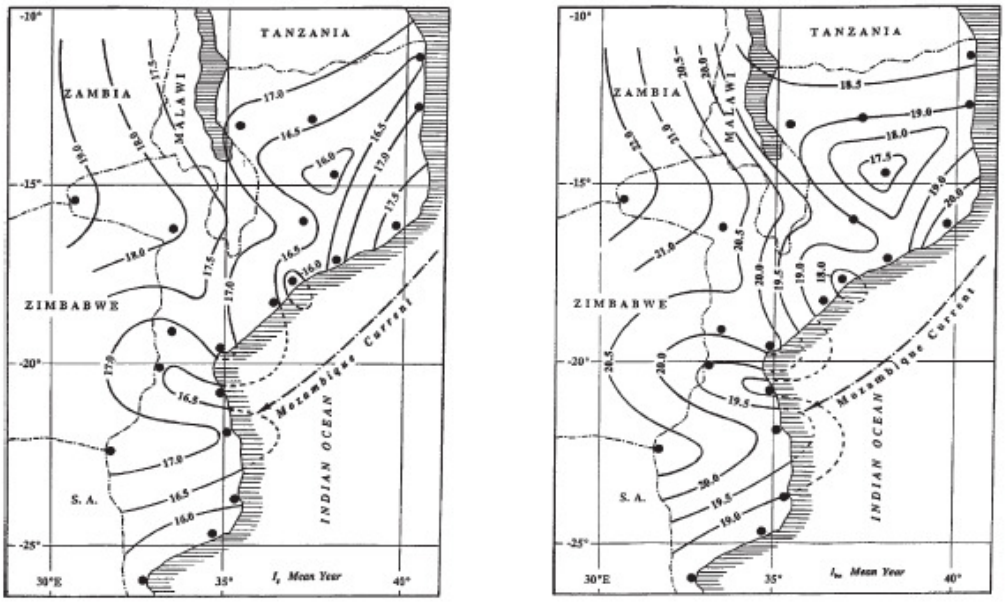

Fig. 5. Maps of annual mean daily global radiation (left) and of annual mean daily direct beam normal radiation (right) for Mozambique. Values indicated are in MJ m^{-2}.

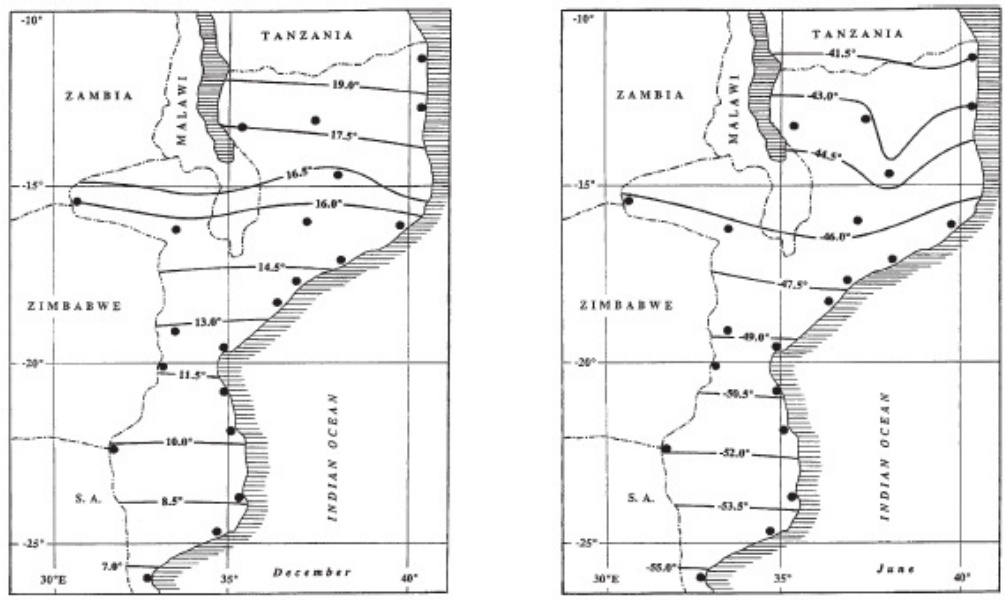

Fig. 6. Maps of monthly mean optimum slopes for December (left) and June (right) for Mozambique.

Table 2
Simulated annual mean daily solar radiation parameters, clearness indices and optimum slopes for 21 synoptic stations of Mozambique

Synoptic station		Clear cloudless conditions					Partly cloudy conditions					$\bar{\beta}^{y}_{opt}$
		$\bar{H}^{y}_{bn}$	$\bar{H}^{y}_{b}$	$\bar{H}^{y}_{d}$	$\bar{H}^{y}_{g}$	$\bar{K}^{y}_{T}$	$\bar{H}^{y}_{bn}$	$\bar{H}^{y}_{b}$	$\bar{H}^{y}_{d}$	$\bar{H}^{y}_{g}$	$\bar{K}^{y}_{T}$	
1.	Angoche	28.5	19.4	3.51	22.9	0.655	20.4	13.8	4.00	17.8	0.484	−19.0
2.	Beira	28.7	19.1	3.50	22.6	0.659	20.1	13.3	3.80	17.1	0.479	−22.5
3.	Chicualacuala	32.0	20.7	3.70	24.4	0.723	20.8	13.2	4.35	17.5	0.494	−25.5
4.	Chimoio	33.0	21.7	3.80	25.5	0.740	20.2	12.8	4.10	16.9	0.479	−22.0
5.	Chinde	28.3	19.1	3.49	22.6	0.652	18.8	12.7	3.90	16.6	0.450	−21.0
6.	Errego	32.0	21.5	3.73	25.2	0.720	19.0	12.7	4.10	16.8	0.450	−18.5
7.	Espungabera	33.1	21.7	3.75	25.4	0.741	19.5	12.6	4.00	16.6	0.462	−23.5
8.	Inhambane	29.0	18.9	3.49	22.4	0.666	19.0	12.3	3.90	16.2	0.460	−27.0
9.	Lichinga	35.4	23.7	3.89	27.6	0.780	19.3	12.8	4.10	16.9	0.454	−15.5
10.	Maputo	29.1	18.6	3.49	22.1	0.670	18.8	11.8	4.11	15.9	0.460	−29.5
11.	Marrupa	33.4	22.6	3.82	26.4	0.746	19.0	12.7	4.00	16.7	0.455	−15.0
12.	Mocimboa da Praia	28.5	19.8	3.53	23.3	0.655	18.3	12.6	3.90	16.5	0.493	−13.0
13.	Nova Mambone	29.1	19.3	3.53	22.8	0.668	19.0	12.3	4.15	16.4	0.456	−24.0
14.	Pebane	28.3	19.2	3.49	22.7	0.653	19.1	13.0	3.80	16.8	0.458	−20.0
15.	Pemba	28.4	19.6	3.52	23.1	0.653	19.0	13.1	3.90	17.0	0.455	−15.0
16.	Quelimane	28.6	19.3	3.51	22.8	0.658	18.0	12.1	3.70	15.8	0.435	−20.5
17.	Quissico	29.1	18.8	3.49	22.3	0.669	18.3	11.8	4.10	15.9	0.445	−28.0
18.	Ribaue	32.3	21.8	3.75	25.5	0.726	17.1	11.7	4.10	15.8	0.408	−17.0
19.	Tete	31.4	21.1	3.72	24.8	0.711	20.9	14.0	4.10	18.1	0.494	−19.0
20.	Vilanculos	28.6	18.9	3.50	22.4	0.662	19.9	13.0	3.90	16.9	0.475	−25.0
21.	Zumbo	31.8	21.4	3.70	25.1	0.718	22.4	17.9	4.30	19.2	0.527	−18.0
Country average		30.4	20.3	3.61	23.9	0.692	19.4	12.8	4.00	16.8	0.465	

4. Results and discussion

4.1. Maps of monthly mean daily direct normal solar radiation for Mozambique

Since knowledge of monthly mean daily direct normal components are important for designing solar devices that can be adjusted for monthly changes in solar conditions, it is useful to produce maps of $\bar{H}_{bn}$ for Mozambique. Such maps are highly valuable since they allow the estimation of $\bar{H}_{bn}$ for any location by extrapolation. Figs 4–6 were produced manually by joining points of the same value. The changes in solar parameters between neighboring synoptic station were simulated by changing location parameters and by extrapolating meteorological data. Fig. 4 shows maps of $\bar{H}_{bn}$ for December and June. Two main principles were used while producing these maps: (i) isoinsolation curves should not cross one another and (ii) the curves should be smooth, without sharp turns. It was necessary to make some simulations in between neighbouring stations while producing these maps. In these cases meteorological parameters were found by extrapolation. Comparing the maps for December and June it can be seen that they are completely different and very complicated. In June there are several notable locations such as Ribaue, Quelimane, Vilanculos and Quissico. Ribaue is of particular note. Moving from Angoche to Lichinga via Ribaue in June, one would find $\bar{H}_{bn}$ first decreases from 19.0–12.2 MJ/m^2 (Ribaue) and then increases to 21.5 MJ/m^2 at Lichinga. It is clear from these data that the weather at Ribaue is much cloudier. Careful analysis shows that the number of h of cloud in June and December, at different locations, is correlated with the prevailing trade winds blowing in Mozambique during these months. The southeasterly winds that blow in Mozambique in June are quite shallow and so are affected by mountain ranges. The streams of trade winds blowing from the southeastern region of the Mozambique Current, over Chinde and Quelimane (another notable location) are affected by the Maniamba–Amaramba Mountains and so clouds concentrate over the Ribaue region. In the south, the southeasterly winds are affected by the Libombos mountain range in Maputo province. In the southern part of Mozambique isoinsolation $\bar{H}_{bn}$ curves almost coincide with the direction of the prevailing winds. Isoinsolation curves for the month of December are determined, to a large extent, by the prevailing trade winds blowing from the northeast. The highest insolation (20.4 MJ/m^2) is at Vilanculos. The only explanation of this fact is the Mozambique Current, which flows from the Indian Ocean straight to Vilanculos. The whole region of Mozambique from Maputo to Beira is under the influence of this warm current. Excepting Vilanculos, there are two other notable locations on the December map: Beira and Lichinga stations. Again, this could be explained by the increased amount of cloud at Lichinga compared to Beira. Moving from Beira ($\bar{H}_{bn}$=19.7 MJ/m^2) to Chimoio ($\bar{H}_{bn}$=17.5 MJ/m^2), $\bar{H}_{bn}$ is seen to decrease (see Fig. 4). The amount of cloud increases from Beira to Chimoio. In June, $\bar{H}_{bn}$ is very high at Zumbo (23.9 MJ/m^2) but is much lower in December (17.7 MJ/m^2). This apparently surprising observation is again explained by the amount of sunshine in the Zumbo area: in June there are 9.1 h of sunshine while in December, only 6.5 h. The difference between S/S_{max}, the fraction of daylight h that are cloudless, for June and December is quite

large. Thus, one can conclude that maps of $\bar{H}_{bn}$ for June and December have special characteristics that are determined by the prevailing trade winds, the warm Mozambique Current and the mountain chains surrounding Mozambique from the north, west and southwest. For completely clear, cloudless weather, the annual mean $\bar{H}_{bn}$ is highest (see Table 2) at Lichinga ($\bar{H}_{bn}$=35.4 MJ/m^2), which is explained by the altitude (A=1356 m).

4.2. Maps of annual mean daily direct beam and global solar radiation

In order to estimate the annual mean values of H_{bn} and H_g at any location, maps of the annual values have been produced for Mozambique (Fig. 5). Again one can see that Ribaue is a special case where $\bar{H}^y_{bn}$ and $\bar{H}^y_g$ are at their lowest. The maps for $\bar{H}^y_{bn}$ and $\bar{H}^y_g$ have the same character and four special areas can be identified in Mozambique. The first area is around Ribaue, where clouds are concentrated around that station. The second area is located along the Zambezi river valley where the solar radiation steadily increases from Quelimane and Chinde stations towards Zumbo station. The third area is that between Vilanculos and Beira stations where the amount of radiation is relatively low and slowly increases from Beira in the direction of Espungabera. The fourth area stretches from Maputo northward to Vilanculos. In this area the amount of solar radiation increases slowly from Maputo in the direction of Chikualacuala. In the northwestern part of Mozambique and also in Malawi and the eastern part of Zambia the isoinsolation lines follow the direction of the prevailing trade winds. Analysis of these maps allows the conclusion that all of the isoinsolation curves are determined by the number of h of sunshine, which, in its turn, is determined by the clouds carried by the trade winds and the mountain chains. If monthly mean monthly daily components were simulated for more stations in neighbouring countries then it is possible that the maps may be slightly altered, but only beyond the borders of Mozambique. More simulations must be carried out for synoptic stations in Tanzania, Zambia, Zimbabwe and South Africa to extend the maps of Mozambique to the neighbouring countries. There are three climate zones in Mozambique: (1) rainy in the north, (2) drier in the south and (3) relatively cool and rainy on the plateaux, mountains and central area. All three zones can be easily traced on the maps of the annual mean solar radiation parameters for Mozambique in Fig. 5. The two maps are correlated to a large extent, which is unsurprising since the greatest contribution to H_g is H_b—the beam component on the horizontal surface. The importance of annual mean solar radiation maps is discussed by Rabl [18].

4.3. Maps of monthly mean optimum slopes

Maps of monthly mean optimum slopes for December (left) and June (right) are presented in Fig. 6. The the mean monthly slopes in this work are defined as follows. If γ=0 (collector faces South) then β changes within $0 \leq \beta \leq 180°$, but if γ=180° (collector faces North) the β changes within $0 \geq \beta \geq -180°$. As one can see in this figure, the monthly mean slopes for December are positive (collector facing South)

and vary from 7° (at Maputo) to 19° (in the northern part of Mozambique). The monthly mean optimum slopes for June are negative (collector facing North) and vary from −55° (Maputo) to −41.5° (Mocimboa da Praia). Once again Ribaue is a notable location. The curves linking similar optimum slopes are bent towards greater tilt angles around the Ribaue area. This is especially evident for the month of June. Such behaviour of the curves is explained by the amount of cloud, which is higher at Ribaue than anywhere else. The mean monthly optimum slope at Ribaue in June should be −44.7° for clear weather, but due to the cloudy conditions it is actually −43°. Hence, the optimum slope is decreased due to the higher cloud cover. This is quite clear from a physical point of view. In a completely cloudy sky the optimum slope would have to be 0° in order to intercept all diffuse radiation. In December the Ribaue area is less cloudy and so the optimum slope curves are less deformed in this area than for June. Such maps of monthly mean optimum slopes can be made for every month of the year. These maps are of great importance: for example, if the angle of tilt of a PV-panel were to be corrected once a month then the efficiency of the panel would be boosted by 15% at little additional cost [19].

4.4. Variation of optimum slope with days of the year

The optimum slopes for Maputo shown in Table 1 are simulated for the Julian days, Jan 17, Feb 16, Mar 16, Apr 15, May 15, June 11, July 17, Aug 16, Sep 15, Oct 15, Nov 14, Dec 10. Using values of monthly mean optimum slopes one can plot the variation of daily optimum slope with day of the year. Such graphs for Maputo and Mocimboa da Praia stations are given in Fig. 7. From this figure it can be seen that the variation of β_{opt} resembles a cosine function. These smooth curves are for clear, cloudless weather conditions. For partially cloudy conditions the curves would be slightly different. Looking at the graph it can be seen that the slopes can assume either negative (North facing) or positive (South facing) values. One can also conclude that the annual mean optimum slope should be negative. The shaded area shows the manifold of positive and negative slopes of an absorber plate for different cloud conditions. As an example, at the Maputo station the slopes are North facing from February to October and only from November to January should the absorber face South. Again, for Maputo, the maximum North facing optimum slope is −55.8° (on 21st June) while the maximum South facing optimum slope is 7.1° (on 21st December). For Mocimboa da Praia the picture is very different. The positive shaded area is greater for Mocimboa da Praia than for Maputo and the negative shaded area is less. Thus, for Mocimboa da Praia, the maximum value of the optimum slope facing North is −44.0° on June 21st (less than for Maputo) and facing South is 22.0° on 21st December (greater than for Maputo). This can only be explained by the difference in latitudes, since the optimum slope is mostly determined by the latitude [14].

4.5. Variation of hourly solar radiation components with time of day

Fig. 8 gives an example of the variation of the hourly solar radiation components for the Maputo station on the 21st June and 21st December during winter and sum-

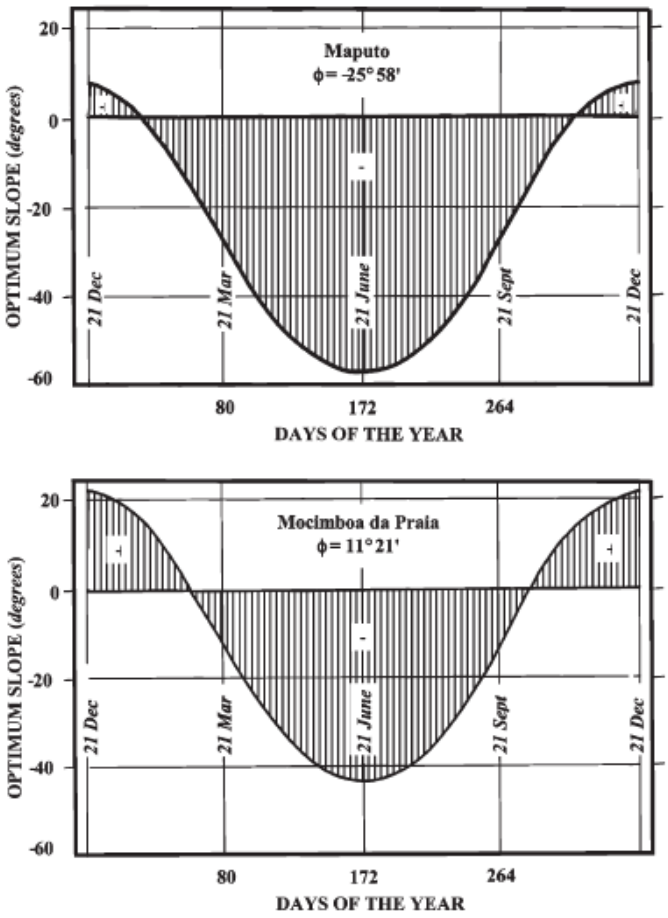

Fig. 7. Variation of optimum slope with days of the year for the Maputo (top) and Mocimboa da Praia (bottom) locations in Mozambique.

mertime, respectively. From the curves it can be seen that in both June and December, the solar radiation is symmetrically distributed over the day, the highest value being at solar noon (no phase shift). All the graphs show that the normal beam radiation, I_{bn} at sunrise and sunset is not equal to zero. This is due to the effect of air mass, which is non-infinite at the hour of sunrise and sunset [13]. The curves also show that the solar radiation components have their highest values in December (summer) rather than in June. The direct normal beam radiation, I_{bn}, is greater than the global radiation, I_g (where I_g is on the horizontal plane) in almost all cases. However, in December, symmetrically and close to the solar noon I_g becomes larger than I_{bn}. This is due to the influence of the zenith angle θ_z on the beam radiation I_b. The graphs in Fig. 8 are obtained for monthly mean meteorological conditions in June and December. In reality however, the humidity in Mozambique can vary from 30–100%. Hence the spread of the hourly solar radiation components could be

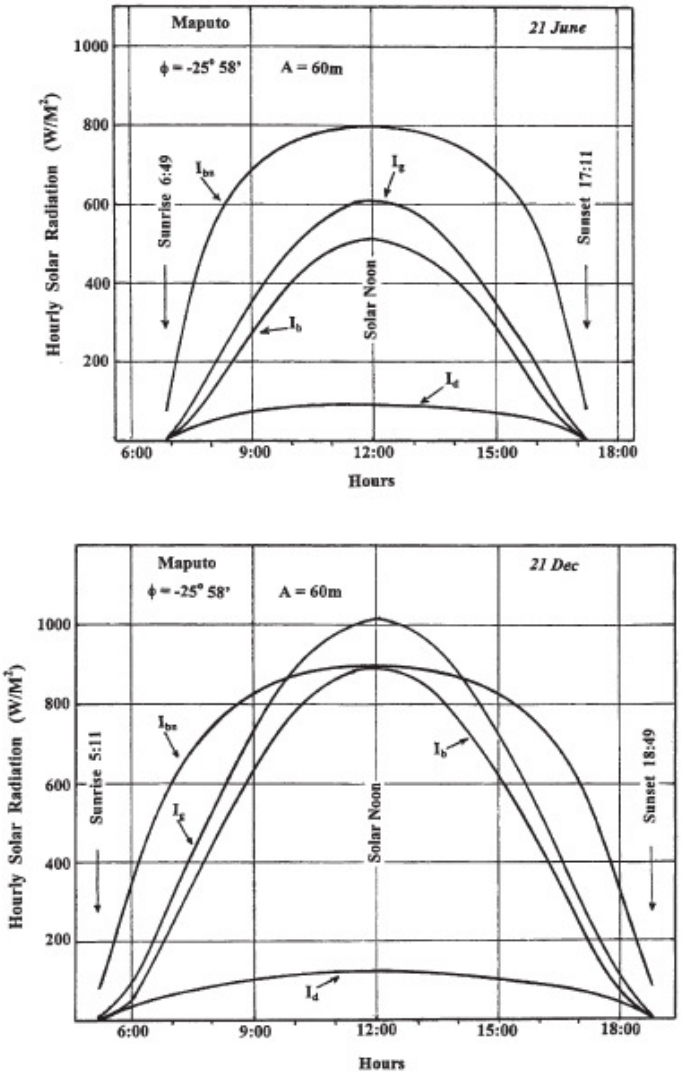

Fig. 8. Variations of hourly solar radiation with time of day (from sunrise to sunset) for Maputo. Top, 21st June, Bottom, 21st December.

within ±20%. At solar noon in December, direct beam radiation in the southern province of Mozambique could be as high as 1070 W/m^2 and could approach 1200 W/m^2 at Lichinga (due to the altitude).

4.6. Variation of monthly mean daily Solar components with days of the year

Examples of the variation of monthly mean daily solar components with day of the year for the Maputo, Lichinga and Mocimboa da Praia locations are given in

Fig. 9. These curves are simulated for clear, cloudless conditions. As can be seen in this figure, H_{bn} H_b, H_g and H_d are smooth curves but are not symmetric about 21st June. The distortion from symmetry is explained by the variation of monthly mean meteorological parameters (T, RH) which affect the solar components. The absolute values of H_{bn}, H_b and H_g for Lichinga are much higher than for Maputo and Mocimboa da Praia. This is explained solely by the differences in altitude. The same graphs can be produced for partially cloudy weather (for real monthly mean meteorological conditions). However, such graphs would not be smooth since the number of h of sunshine, S, changes more randomly than temperature or humidity: S is determined by the cloud-cover, while T and RH are determined mostly by the seasons.

4.7. Annual mean solar radiation parameters and annual mean optimum slopes of Mozambique

Table 2 represents all annual mean solar radiation parameters ($\bar{H}^y_{bn}\bar{H}^y_b\bar{H}^y_d\bar{H}^y_g$), annual mean clearness indices, $\bar{K}^y_T$ and annual mean optimum slopes, β^y_{opt} for 21 locations of Mozambique for clear, cloudless and for partially cloudy weather (monthly mean meteorological conditions). Analysis of Table 2 allows the conclusion that all solar radiation components for clear, cloudless weather are quite high. $\bar{H}^y_{bn}$ varies between 28.3 MJ/m^2–35.4 MJ/m^2, the country average being 30.4 MJ/m^2. The country average of $\bar{H}^y_g$ is also quite high (23.9 MJ/m^2). The average clearness index is 0.692. For partially cloudy conditions $\bar{H}^y_{bn}$ and $\bar{H}^y_g$ are less but the values are still quite high. Country average values for partially cloudy conditions are 19.4 MJ/m^2 and 16.8

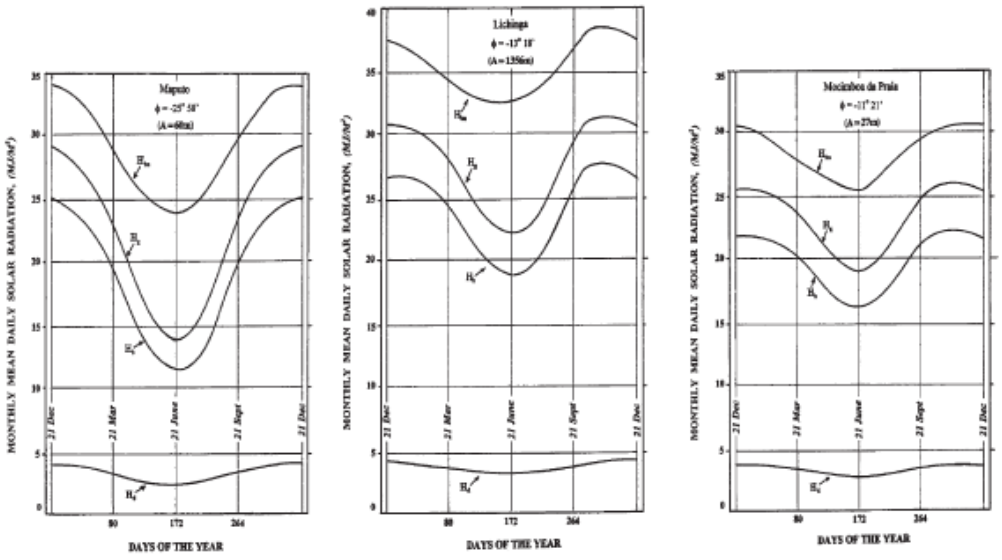

Fig. 9. Variation of monthly mean daily solar radiation components for the Maputo (left), Lichinga (centre) and Mocimboa da Praia (right) locations of Mozambique (monthly mean meteorological parameters were used in the simulations).

MJ/m^2, respectively. Annual mean optimum slopes, $\bar{\beta}^y_{opt}$ (°) given in the right hand column of Table 2, are all negative. Values of $\bar{\beta}^y_{opt}$ are found as follows. Yearly H^y_T values were simulated as $\Sigma^{365}_{n=1} H_T(n)$ for different values of β until maximum H^y_T is found [11]. The corresponding value of β would be the mean year optimum slope.

Careful theoretical consideration of this problem, carried out using special software [11], showed that for the Southern African region (SADC countries) the following empirical formula can be used to calculate $\bar{\beta}^y_{opt}$:

$$\bar{\beta}^y_{opt} = \frac{\beta_{opt}(21\ \text{June}) + \beta_{opt}(21\ \text{December})}{2} + \frac{\varphi}{5}. \tag{4}$$

As an example, for Maputo this formula gives:

$$\bar{\beta}^y_{opt}(\text{Maputo}) = \frac{-55.8 + 7.1}{2} - \frac{26}{5} = -29.5°.$$

Annual mean optimum slopes $\bar{\beta}^y_{opt}$ for clear, cloudless and partially cloudy weather are practically the same (see Table 1). Hence, in the Southern African region, where monthly mean cloudy h are quite low, values of $\bar{\beta}^y_{opt}$ for clear, cloudless weather can be used throughout the year.

5. Conclusions

1. Maps of monthly mean daily direct normal insolation for June and December and maps of the annual mean direct normal and global insolation show that the behaviour of the isoinsolation curves is affected, to a high degree, by the prevailing trade winds and mountain chains of Mozambique.
2. Maps of the annual mean daily direct normal and global insolation components produced for Mozambique can be used to design the size and to estimate the cost and efficiency of different solar devices.
3. Annual mean optimum slopes simulated for 21 Mozambican synoptic stations can be used in the installation of PV-arrays and plane collectors at different locations. Monthly mean optimum slopes could be of especial importance if PV-arrays were designed and manufactured so as to allow adjustment of the optimum slope of the array whenever necessary (e.g. once a month)
4. To produce more precise maps of the solar insolation components for Mozambique and neighbouring countries, more simulations for synoptic stations of neighbouring countries should be conducted.
5. Mozambique is a very suitable country to utilize direct beam radiation since H_{bn} values are high and do not vary much throughout the year. For example, at Maputo the lowest value of H_{bn} is 16.6 MJ/m^2 in November and the highest is 20.4 MJ/m^2 in August (see Table 1). The annual mean value of H_{bn} is 18.8 MJ/m^2.
6. The H_g component is also quite high throughout Mozambique and can be effectively used for heating domestic water and for communication purposes if PV-arrays are used. The annual mean value of H_g for Mozambique is 16.8 MJ / m^2.

References

[1] Duffie JA, Backman W, Solar Engineering of Thermal Processes, 2nd ed. John Wiley and Sons, New York 1991 (pp. 46-141).
[2] Löt GOG, Tybout RA. Cost of house heating with solar energy. Solar Energy 1973;14:253.
[3] Kern J, Harris L. On the optimum tilt of a solar collector. Solar Energy 1975;17:97.
[4] Iqbal M. Optimum collector slope for residential heating in adverse climates. Solar Energy 1979;22:77.
[5] Lunde PJ, Solar Thermal Engineering, Wiley, New York 1980.
[6] Garg HP, Treatise on Solar Energy, Vol 1: Fundamentals of Solar Energy, Wiley, Chichester 1982 (p 378).
[7] Terjung WH, O'Rourke PA. A worldwide examination of solar-beam slope angle values. Solar Energy 1983;31:217.
[8] Koronakis PS. On the choice of the angle of tilt for south facing solar collectors in the Athens basin area. Solar Energy 1986;36:217.
[9] Chiou JP, El-Naggar MM. Optimum slope for solar insolation on a flat surface tilted towards the equator in heating season. Solar Energy 1988;36:471.
[10] Elsayed MM. Optimum orientation of absorber plates. Solar Energy 1989;42:89.
[11] Nijegorodov N, Devan KRS, Jain PK, Carlsson S. Atmospheric transmittance models and an analytical method to predict the optimum slope of an absorber plate, variously oriented at any latitude. Renewable Energy 1994;4:529–43.
[12] Nijegorodov N. Analytical models and new algorithm to simulate solar radiation components and optimum slope of an absorber plate variously orient at any location. In: Proceedings of ISES World Congress. 1999.
[13] Nijegorodov N, Luhanga PVC. Air mass: analytical and empirical treatment; an improved formula for air mass. Renewable Energy 1996;7:57–65.
[14] Nijegordov N, Adedoyin JA, Devan KRS. A new analytical–empirical model for the instantaneous diffuse radiation and experimental investigation of its validity. Renewable Energy 1997;11:341–50.
[15] Nijegordov N, Luhanga PVC. A new model to predict direct normal instantaneous solar radiation, based on laws of spectroscopy, kinetic theory and thermodynamics. Renewable Energy 1998;13:523–30.
[16] Kasten F. A new table and approximate formula for relative optical air mass. Arch Meteorol Geophys Bioklimatol Ser 1966;B14:206–23.
[17] Van Heuklon TK. Estimating the atmospheric ozone for solar radiation models. Solar Energy 1979;22:63–8.
[18] Rabl A, Active Solar Collectors and their Application. Oxford University Press, New York 1979 (pp. 48-75).
[19] Nijegorodov N, Jain PK. Optimum slope of a north–south aligned absorber plate from the north to the south poles. Renewable Energy 1996;11:107–18.